Journal of The Electrochemical Society, **160** (9) C445-C450 (2013)
0013-4651/2013/160(9)/C445/6/$31.00 © The Electrochemical Society

In-Situ XAS Investigation of the Effect of Electrochemical Reactions on the Structure of Graphene in Aqueous Electrolytes

Juan J. Velasco-Velez,[a] Cheng-Hao Chuang,[b,c] Hui-Ling Han,[d] Inigo Martin-Fernandez,[e,g] Camille Martinez,[a,f] Way-Faung Pong,[c] Yuen-Ron Shen,[d] Feng Wang,[d] Yuegang Zhang,[e,*,h] Jinghua Guo,[b] and Miquel Salmeron[a,f,z]

[a]*Materials Science Division, Lawrence Berkeley National Laboratory, Berkeley, California 94720, USA*
[b]*Advanced Light Source, Lawrence Berkeley National Laboratory, Berkeley, California 94720, USA*
[c]*Department of Physics, Tamkang University, Tamsui, Taiwan 251*
[d]*Department of Physics, University of California Berkeley, Berkeley, California 94720, USA*
[e]*The Molecular Foundry, Lawrence Berkeley National Laboratory, Berkeley, California 94720, USA*
[f]*Materials Science and Engineering Department, University of California Berkeley, Berkeley CA 94720, USA*

In-situ X-ray Absorption Spectroscopy (XAS), Raman Spectroscopy, AFM and XPS have been used to investigate the effect of reactions occurring in aqueous electrolytes on the structure of a single-layer graphene produced by CVD. It was found that defects are readily and irreversibly produced by application of electrode voltages. The defects and the products were identified also by new features in the XAS spectra. Our findings show the poor stability of the CVD graphene, which could be a challenge in applications such as super-capacitors, fuel-cells, batteries and photo-catalysis.
 [DOI: 10.1149/2.113309jes]

Manuscript submitted February 6, 2013; revised manuscript received July 9, 2013. Published July 17, 2013.

Graphene has become a major topic of research because of its unique electronic and chemical properties.[1–4] Desirable properties of graphene include high mechanical strength, good thermal and electrical conductivity and chemical stability in aggressive media. In addition graphene can be functionalized to increase its chemical selectivity in catalysis and sensing applications. However these properties can be strongly modified by the presence of defects. In applications to electronic devices for example, defects and functional groups of adsorbed molecules influence the electronic and transport properties.[5] While the chemistry of defects on graphite has been investigated extensively,[6] their nature is still under debate. One popular method to produce graphene is through chemical vapor deposition (CVD), which produces polycrystalline sheets of variable quality, determined by the density of grain boundaries, point defects and chemical contamination.

A variety of characterization techniques have been used to investigate the properties and structural perfection of graphene, including scanning tunneling microscopy (STM),[7] Raman spectroscopy,[8] X-ray photoemission spectroscopy (XPS),[9] X-ray absorption spectroscopy (XAS) and X-ray emission spectroscopy (XES).[10–14] Traditionally, XAS measurements of graphene have been carried out in ultra-high vacuum (UHV), which drastically limits the type of environments that can be investigated. To perform the more desirable in situ experiments we have developed electrochemical cells specifically designed for in situ XAS/XES measurements under ambient conditions. The experiments were carried out in beamline 8.0.1 of the Advanced Light Source (ALS) at the Lawrence Berkeley National Laboratory (LBNL). The cells were first demonstrated in a study of the electrochemical oxidation and reduction of Cu[15–17] where the fluorescence detection mode was used. While this is appropriate for studies of the chemistry of the electrode materials, the signal obtained is bulk sensitive due to the large penetration depth of soft X-rays (∼μm). Using total electron yield detection (TEY) however, we can obtain information of the interface region due to the much shorter mean free path of the secondary electrons (∼nm), which make possible studies of the Helmholtz layer region. In our cell the detection of the TEY current is made in the same working electrode under study.

In the experiments reported here the electrode consists of a CVD grown single graphene layer (SGL), wet-etched and transferred onto a 100 nm thick Si_3N_4 membrane with an X-ray transmission of 46% at the C K-edge (285 eV) and 66% at the O K-edge (530 eV). This membrane is used to separate the electrochemical cell from the vacuum chamber connected to the Synchrotron ring, as illustrated in Figure 1. The cell contains Pt and Ag wires that act as counter and reference electrodes respectively. By the use of a micro-pump the electrolyte is flown through inlet and outlet holes, which helps eliminate possible bubbles and also drains away ionized species from the electrolyte. The potential is controlled with a potentiostat which is used to record I-V cyclic voltamograms (CV), and chrono-amperometric (CA) measurements. Using this experimental setup, it is possible to achieve real time monitoring of the element-specific electronic structure changes in situ after electrochemical cycling.

The chemical composition of the samples was characterized ex-situ using XPS, Raman spectroscopy, and Atomic Force Microscopy (AFM). Raman spectroscopy is used extensively to characterize the degree of perfection of graphene through the relative changes in the Raman peak intensities, some of them characteristic of particular types

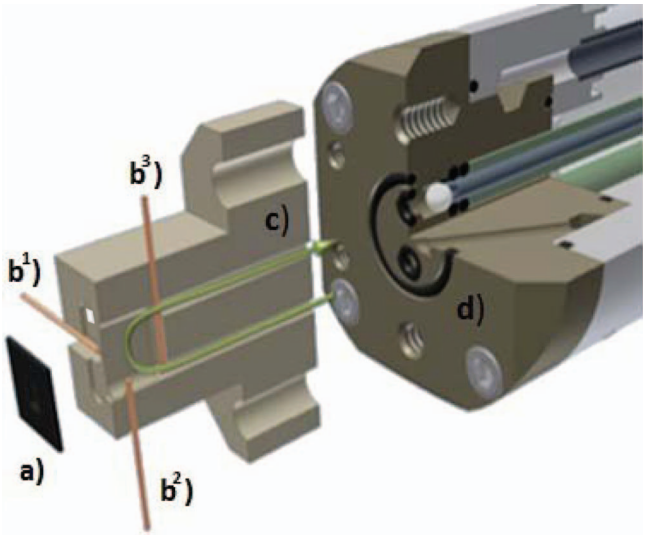

Figure 1. Schematic drawing of the electrochemical cell used in this study. a) thin (∼100 nm at the center) Si_3N_4 membrane with the working electrode (graphene) coating the back side); b^1) working electrode contact; b^2) reference electrode (Ag wire); and b^3) counter electrode (Pt wire). d) Main body of the liquid cell. The green line represents the electrolyte flow.

*Electrochemical Society Active Member.
[g]Present address: National University of Singapore (NUS), Singapore 11754, Singapore.
[h]Present address: Suzhou Institute of Nano-Tech and Nano-Bionics, Chinese Academy of Sciences, Suzhou 215123, China.
[z]E-mail: mbsalmeron@lbl.gov

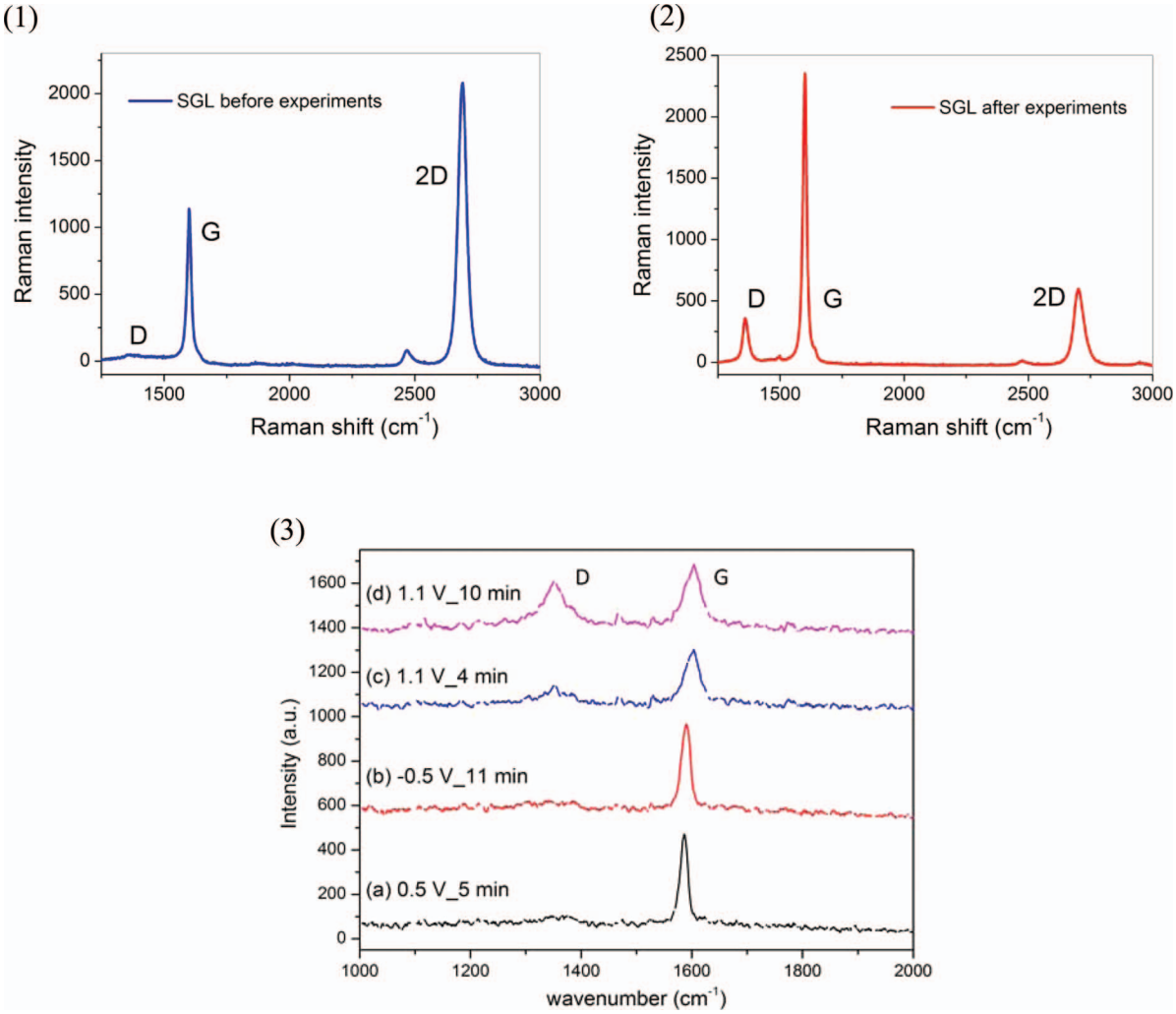

Figure 2. Raman spectra of a single graphene layer sample (1) before and (2) after the electrochemical experiments consisting of 100 CV cycles between –1 V to +1 V at 100 mV/s starting and finishing at 0 V, followed by a 5 minute CA at –1 V and 5 minute CA at +1 V. (3) In situ Raman spectra acquired at the indicated bias voltage for graphene samples in 2 mM NaCl. The spectra show the irreversible growth of the D band at positive bias higher than 1 V. The laser wavelength used during the measurements was 520 nm.

of defects.[18] The most intense ones being the G peak at ∼1580 cm^{-1} due to the in-plane vibration mode of the graphitic lattice, and the 2D peak at ∼2700 cm^{-1} due to the excitation of two phonons with opposite momentum in the highest optical branch and sensitive to the number of graphene layers (Figure 2).[19] The peak at ∼1350 cm^{-1} or D peak is related to lattice point defects. Another peak at ∼1500 cm^{-1} (D^{**}) is sometimes present that has been attributed to a highly disordered and wrinkled morphology.[20]

All electrochemical experiments in this work were performed in a 2 mM NaCl solution, with voltages relative to a Ag/AgCl reference. All CV measurements are closed cycles starting and finishing at 0 V, at a rate of 100 mV/sec.

Sample preparation and characterization

The SGL sample was grown on a copper foil by chemical vapor deposition (CVD) using methane at 1000°C following a procedure described in reference.[21] A 500 nm thick layer of polymethylmethacrylate (PMMA) was spin-coated on top of the graphene, followed by the removal of copper by wet etching (∼30% $FeCl_3$ and ∼4% HCl in deionized water). The SGL was then transferred onto the Si_3N_4 membrane window and onto Si/SiO_2 wafer substrates. Finally the PMMA was removed with acetone and the substrate cleaned with isopropanol. It has been found that ripples and wrinkles can be formed due to uneven attachment of the SGL to the SiO_2 substrate during the transfer process.[22,23] The CVD grown graphene is polycrystalline, with crystallite sizes in the micro-meter range.

The sample was characterized by Raman spectroscopy using laser light of 520 nm wavelength (Horiba LabRAM ARAMIS). Results for a sample transferred onto a Si/SiO_2 substrate are shown in Figure 2.1. The 2D/G peak intensity ratio is ∼2, the full width at half maximum (FWHM) of the 2D band is <40 cm^{-1}, and the intensity of the D band is negligible. These measurements indicate that the SGL has a low defect concentration over the entire layer except at the edges and around visible defective areas.

AFM images acquired before the electrochemical experiments (Figure 3a) show again that the initial graphene layer presents a low concentration of defects.[22,23] The ripples and tears visible in the image separate domains of micrometer size, so that the number of defects, low coordinated edge atoms in particular, is relatively low. The chemical composition and in particular the possible presence of Cu impurities from the etching process was checked by XPS. The spectrum in Figure 4 shows peaks at 535 eV, 285 eV, 150 eV and 99 eV, which correspond to O, C, and Si respectively. No indication of Cu contamination above the detection limit of approximately 0.1% of a monolayer was found.

The chemical and electronic structure of graphene in contact with the NaCl aqueous solution was studied in situ by (XAS). The spectra

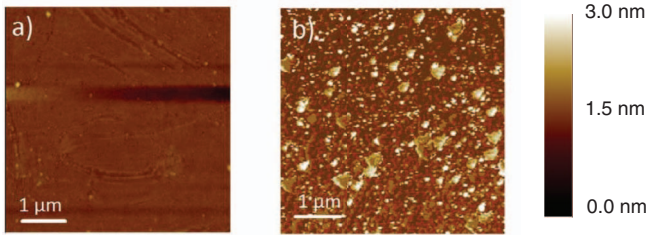

Figure 3. AFM images of a wet transferred single layer graphene deposited on a SiO_2/Si wafer under ambient conditions: a) Topographic AFM image before the electrochemical experiments, showing relatively large homogeneous regions. b) AFM image after electrochemical experiments (100 scans from −1 V to +1 V).

were acquired in the total electron yield mode using the SGL electrode to collect the current with a resolution of 0.1 eV. The spectra were normalized to the incident beam intensity measured upstream of the experimental chamber. The acquisition time for each spectrum was about 25 minutes. No beam damage was detected in the experiments as checked by repeated consecutive scans. The spectra were normalized to the adsorption pre- and post- edges and calibrated using a HOPG reference sample situated in the ultra-high vacuum chamber.[24] The C K-edge XAS spectra are shown in Figure 5: The top curve shows a reference HOPG spectrum recorded in UHV, the second is from a SGL in UHV, the third corresponds to a SGL in contact with the electrolyte, the fourth is from acid-treated graphene oxide (A-GO), in 2 $KMnO_4$: 3 H_3PO_4. Finally the bottom curve is from an amorphous carbon (AC) film in vacuum. The main XAS spectral features in these spectra are related to graphitic π^* and σ^* LUMO electronic states, which correspond to the peaks at 285.5 eV and 291.5 eV.[24,25] Both peaks are characteristic signatures of graphitic samples. When in contact with 2 mM NaCl aqueous electrolyte the graphene spectra is characterized by a change in the ratio π^* to σ^* peaks indicative of distortion of the sp^2 configuration to a more sp^3-like configuration,[26] i.e., becoming more amorphous as we can see by simple comparison in Figure 5. The peaks at the position marked by the C and D lines are related to the presence of C-OH and COOH groups.[27–29]

Electrochemical Measurements

The stability of a CVD grown SGL was investigated after several CV cycles between −1 and +1 V, as shown in Figure 6. In the first cycle a small peak appeared at +0.1 V due to transient reactions. This peak disappeared in subsequent runs. The CV curves show a flat region

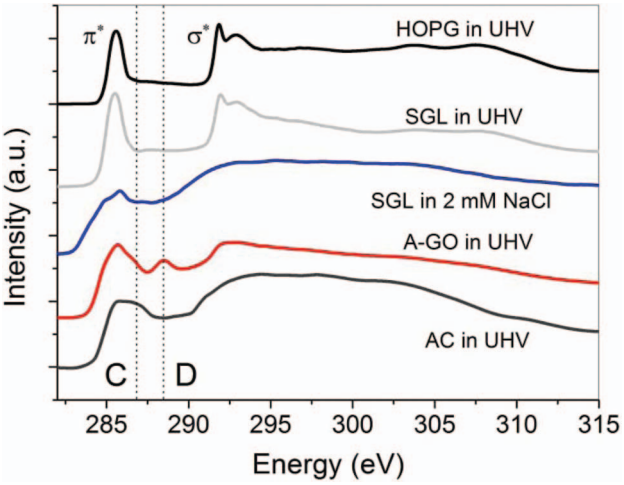

Figure 5. X-ray Absorption Spectra in total electron yield mode collected at the sample electrode. From top to bottom: HOPG sample in UHV, SGL in UHV, graphene in contact with a 2 mM NaCl aqueous electrolyte, acid treated graphene oxide A-GO (2 $KMnO_4$:3 H_3PO_4), and amorphous carbon.

between −0.5 V and +0.5 V, which indicates that no electrochemical reaction takes place in this voltage range at observable rates.

Figure 2.2 shows the Raman spectra after electrochemical experiments consisting of 100 CVs between ±1 V, followed by an additional CA at −1 V during 5 minutes and another at +1 V during 5 minutes. The D/G and 2D/G ratios changed notably, the first increasing and the second decreasing, which is indicative of structural and/or chemical changes. The increase in the intensity of the D band is in line with the large number of fragments observed in the AFM images, as discussed below. Using Cancado et al. equation[30] we estimate the crystallite size to be ten times smaller after the electrochemical experiments. The decrease in the 2D/G ratio is associated to a reduction of graphene quality and consistent with previous oxidation studies of carbon nanotubes.[24,31] The in-situ Raman spectra in Figure 2.3, in a 2 mM NaCl solution, are particularly revealing of the nature of the chemical modifications occurring upon biasing the SGL electrode. Raman spectrum (a) (bottom) shows the absence of defect formation after 5 minutes at +0.5 V. Graphene protonation at low negative potentials can also be discarded, as shown in spectrum (b) (−0.5 V) because no changes were observed in the Raman spectrum after 11 minutes voltage application. However, in electrolytes such as super acids the protonation effects must be considered as a possible source of degradation.[32–34] Finally, potentials beyond +1 V produce an

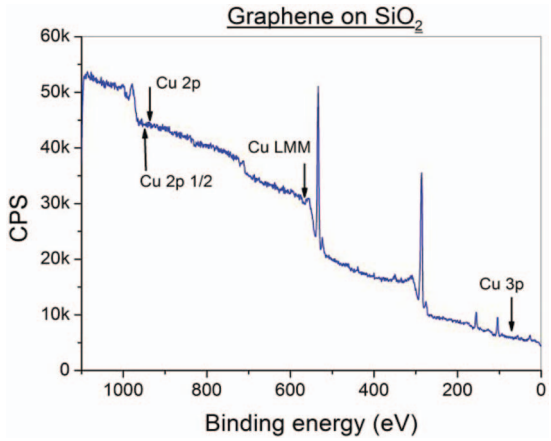

Figure 4. XPS survey of a SGL transferred onto a SiO_2/Si wafer. Copper contamination (expected peaks marked by arrows) is below the detection limit.

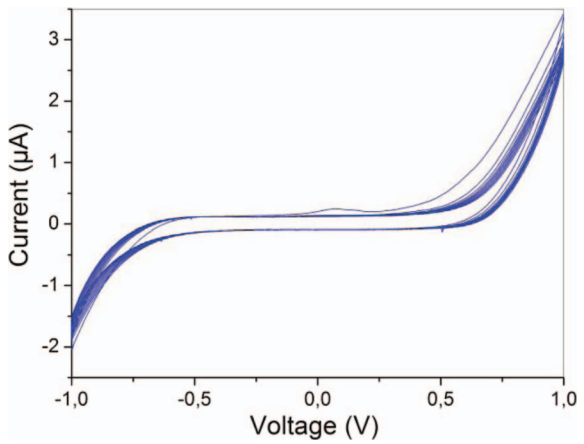

Figure 6. Series of 100 cyclic voltamograms between −1 V and +1 V, scan rate was 100 mV/s. The scan starts and ends at 0 V.

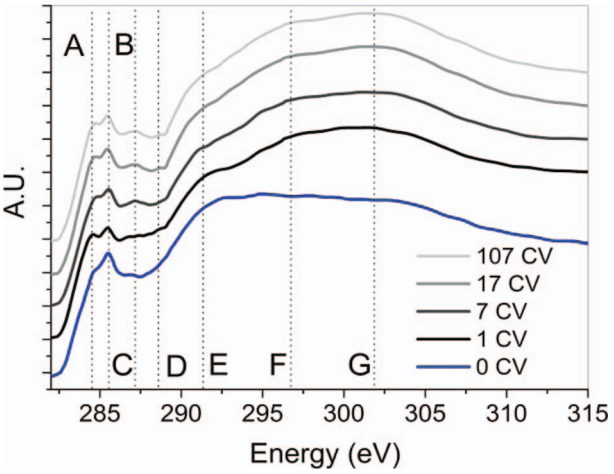

Figure 7. XAS measurements across the C 1s edge of a SGL in aqueous electrolyte (2 mM NaCl) after several CV between −1 V to +1 V, starting and finishing at 0 V (rate scan = 100 mV/s).

increase in the D peak associated with the formation of defects. The intensity of peak D increases with time as shown in spectrum (c) and (d) (after 4 and 11 minutes respectively). Reversing the potential does not restore the original spectra implying that graphene degrades under such conditions. The AFM images acquired after the electrochemical experiments (Figure 3b), clearly show that the graphene layer was severely damaged.

The in situ XAS measurements shown in Figure 7 are more informative of the chemical transformations and the nature of the species adsorbed on the graphene surface. Unfortunately the current implementation of our in situ XAS technique prevents us from collecting spectra while the electrochemical bias is applied. This is because the TEY signal, collected at the same graphene electrode, is superimposed to the large Faradic current between working and counter electrodes which saturates the current pre-amplifier. Therefore the spectra, always collected at 0 V, capture only the irreversible changes in the chemical state of the surface after a complete cycle. The spectra in the figure reveal that after several CV cycles new peaks appear, in addition to the π^* and σ^* peaks of the graphitic state. The new peaks originate from carbon atoms modified by ring opening and by attachment of species such as H, O, OH, etc., as summarized in Table I. One such new feature is the peak labeled A at 284.8 eV,[35,36] which was assigned to the formation of doubly coordinated carbon atoms in open rings, while the peak labeled B at 285.5 eV is assigned to the normal triply coordinated carbon atom in the intact aromatic ring.[27,37,28] The

Table I. Assignment of peak positions and molecular species of carbon K-edge.

Energy (eV)	Electronic transition	Functionality
284.8 (A)	π^*	Doubly coordinated C [35, 36]
285.5 (B)	π^*	Aromatic C [276, 28, 37,]
287.3 (C)	σ^*	C-OH [28]
288.5 (D)	σ^*	COOH [27, 29]
291.5 (E)	σ^*	C = C [29]
296–298 (F)	σ^*	C = O [28]
302.0 (G)	σ^*	C = C [28]

features at 291.5 eV (E), 297.0 eV (F), and 302.0 eV (G) have been associated with $\sigma^*_{C\text{-}C}$, $\sigma^*_{C=O}$ and $\sigma^*_{C=C}$ levels respectively.[28,29] The peak at 287.3 eV (peak C) has been assigned to a σ^* level in C-OH,[28] and that at 288.7 eV (peak D) to the σ^* state of COOH.[27,29] These spectra are similar to that of A-GO (Figure 5), and suggests an increase in the concentration of oxygen species, as well as in the density of defects. This is consistent with the features observed in A-GO marked by dashed lines C and D.

After the initial formation of new defects and species, confirmed by new features (peaks A and C), the SGL remained stable. Its stability after the CVs was investigated at higher potentials following the polarization sequence: +1.5 V, −1.5 V, +2.5 V and −2.5 V. It was found that the graphene layer remains stable at potentials between ±1.0 V vs. Ag as Figure 8b shows. At higher positive potential (+2.5 V) peaks A and C are enhanced, which indicates the occurrence of chemical reactions. On the other hand, the signal is recovered by reversing the potential to −2.5 V although with a substantial decay in the carbon signal. This fact is confirmed by the changes observed in a fresh graphene sample after several CV cycles in the ±2.5 V range are shown in Figure 8a. Two peaks are initially observed near +1.8 V and −1.8 V. The current intensity decreases with the number of cycles, which is likely related to the decay of graphene conductivity as a result of increasing damage from the electrochemical reactions.

Discussion

The results presented in this study indicate the readily occurring degradation of graphene by applied voltages. Figure 6 shows that at potentials between −0.5 V and +0.5 V no peaks are observed in the CV curves, which indicates that electrochemical reaction currents at these low voltages are below the detection limit of ∼nA. An order of magnitude estimate (10^{-9} A × 50 sec ∼ 3 × 10^{11} electrons), over our electrode area of 3 mm^2 indicates that less than 2% of the atoms in the graphene electrode surface were involved at this stage. This is in line

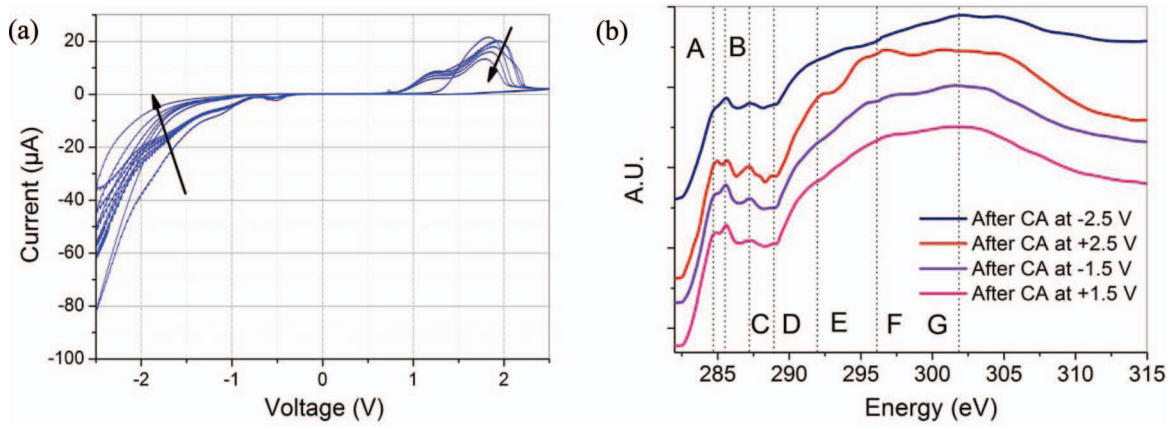

Figure 8. (a) Six cyclic-voltammetry curves from a SGL electrode between −2.5 V and +2.5 V, starting and finishing at 0 V. b) In situ XAS measurements in total electron yield mode collected on the graphene electrode after CA runs at +1.5 V, −1.5 V, +2.5 V and −2.5 V.

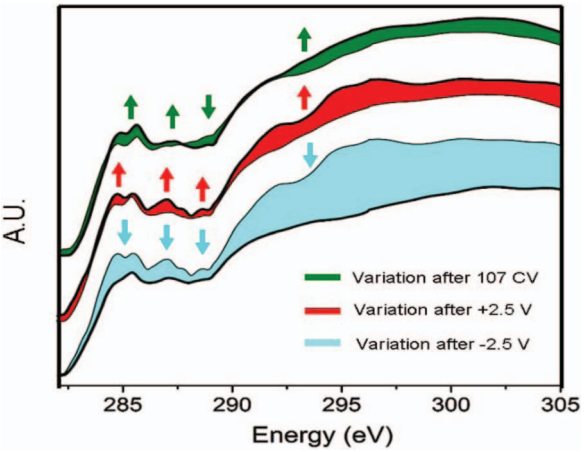

Figure 9. Variations in the XAS after different experiments. Top: after 107 CV. Middle: after a 60 sec CA at +2.5 V. Bottom: after a 60 sec CA at −2.5 V.

with the in situ Raman experiments which showed the SGL stability at low potentials.

The appearance of new peaks in the XAS demonstrates the occurrence of chemical reactions leading to the irreversible formation of species bound to carbon atoms, such as C-OH (peak C), C = O (peak F) and others from COOH dissociation (peak D). The evolution of these peaks is shown in Figure 9 from 1 CV to 107 CVs (green color) between −1 V to +1 V. The arrows indicate an increase in the C and F peaks which we associate to C-OH and C = O, as well as a decrease in peak D, (COOH species). However, after several CV cycles the SGL is stable as the XAS spectra show. Only when the potential is higher than 1.8 V vs. Ag new features appeared in the XAS. For example the spectrum after a 60 second CA pulse at +2.5 V shows an increase in the intensity of peak A, which is characteristic of doubly coordinated carbon atoms in open rings. Similar effects, at potentials beyond the oxidation water potential (more positive than 1.7 V vs. Ag/AgCl, 3M NaCl) have been reported in the electrochemical etching of individual multiwall carbon nanotubes in 0.1 M KCl aqueous solution.[38] This is in line with the AFM measurements after the electrochemical experiments (Figure 3b) which show extensive damage in the form of ruptured graphene, probably along grain boundaries.

Possible reactions between the SGL and the electrolyte at the positive electrode are:[39]

$$C_{x(s)} + H_2O_{(l)} \rightarrow C_xOH_{(s)} + H^+_{(aq)} + e^-$$

$$C - OH_{(s)} \rightarrow C = O_{(s)} + H^+_{(aq)} + e^-$$

$$C = O_{(s)} + H_2O_{(l)} \rightarrow COOH_{(s)} + H^+_{(aq)} + e^-$$

where C-OH groups are produced at positive voltage that could be further oxidized producing C = O and finally COOH groups. This is consistent with the XAS measurements at positive voltage as Figure 8b shows. On the other hand, at negative potential the following reactions are likely to occur:[40]

$$C = O_{(s)} + e^- \rightarrow C - O^-{}_{(s)}$$

$$C = O_{(s)} + H^+_{(aq)} + e^- \rightarrow C - OH_{(s)}$$

which can explain the absence of CO and CH groups observed in Figure 8b.

In summary, the degradation process is presumably due to the formation at positive potentials of C = O, C-OH and COOH. At negative voltages C = O reacts with H^+ to irreversibly produce C-OH groups explaining the appearance of peak C in the XAS at negative voltage (Figure 8b).

Conclusions

By using AFM microscopy, in situ Raman spectroscopy and in situ XAS spectroscopy techniques we have followed the changes in topography, vibrational and electronic structure of SGL electrodes subjected to electrochemical reactions in aqueous electrolyte environments. We have developed in situ XAS recorded in total electron yield mode, which provides interface sensitivity due to the short mean free path of the secondary electrons and thus providing a new tool for spectroscopic studies of electrode/electrolyte (solid/liquid) interfaces. We have demonstrated the potential of the technique in our study of CVD grown graphene, showing that its chemical structure changes appreciably even at potentials below |1| V and increases dramatically at potentials above |1| V. It was found that defects are readily and irreversibly produced by application of electrode voltages. We attribute this to the fact that the CVD graphene contains numerous grain boundaries and various types of the defects. Our results show that the quality of graphene is crucial for applications as super-capacitors, fuel-cells, batteries and photo-catalysis.

Acknowledgments

This was supported by the Office of Basic Energy Sciences, Division of Materials Sciences and Engineering of the U.S. DOE under Contract No. DE-AC02-05CH11231. J.J. Velasco-Velez gratefully acknowledges financial support from the Alexander von Humboldt foundation. Hui-Ling Han is grateful to the National Science Council of Taiwan for financial support under grant No. NSC 100-2917-I-564-048. WFP is grateful to the National Science Council of Taiwan for financial support under grant No. NSC 99-2119-M-032-004-MY3. Experiments at the Advanced Light Source were performed under project #04863.

References

1. A. K. Geim and K. S. Novoselov, *Nat. Mat.*, **6**, 183 (2007).
2. A. H. Castro Neto, F. Guinea, N. M. R. Peres, K. S. Novoselov, and A. K. Geim, *Rev. Mod. Phys.*, **81**, 109 (2009).
3. A. K. Geim, *Sci.*, **324**, 1530 (2009).
4. Y. Zhu, S. Murali, W. Cai, X. Li, J. W. Suk, J. R. Potts, and R. S. Ruoff, *Adv. Mat*, **22**, 3906 (2010).
5. D. A. Areshkin, D. Gunlycke, and C. T. White, *Nano Lett.*, **7**(1), 204 (2007).
6. H. P. Boehm, *Carbon surface chemistry, in Graphene and precursors*. Gordon and Breach Science Publishers, Amsterdam (2001).
7. X. Feng, S. Maier, and M. Salmeron, *J. Am. Chem. Soc.*, **134**, 5662 (2012).
8. E. Pollakt, B. Geng, K.-J. Jeon, I. T. Lucast, T. J. Richardson, F. Wang, and R. Kostecki, *Nano Lett.*, **10**, 3386 (2010).
9. S. S. Chen, L. Brown, M. Levendorf, W. W. Cai, S. Y. Ju, and J. Edgeworth, *ACS Nano*, **5**, 1321 (2011).
10. L. Zhang, E. Pollak, W. C. Wang, P. Jiang, P.-A. Glans, Y. Zhang, J. Cabana, R. Kostecki, C. Chang, M. Salmeron, J. Zhu, and J. Guo, *Carbon*, **50**, 5316 (2012).
11. L. Zhang, N. Schwertfager, T. Cheiwchanchamnangij, X. Lin, P.-A. Glans-Suzuki, L. F. J. Piper, S. Limpijumnong, Y. Luo, J. F. Zhu, W. R. L. Lambrecht, and J.-H. Guo, *Phys. Rev. B*, **86**, 245430 (2012).
12. L. Zhang, L. Ji, P.-A. Glans, Y. Zhang, J. Zhu, and J. Guo, *Phys. Chem. Chem. Phys.*, **14**, 13670 (2012).
13. J.-H. Guo and J. Nordgren, *J. Electron Spectrosc. Relat. Phenom*, **110–111**, 105 (2000).
14. L. Ji, M. Rao, H. Zheng, L. Zhang, Y. Li, W. Duan, J. Guo, E. J. Cairns, and Y. Zhang, *J. Am. Chem. Soc.*, **133**, 18522 (2011).
15. P. Jiang, J. L. Chen, F. Borondics, P. A. Glans, M. W. West, C. L. Chang, M. Salmeron, and J. Guo, *Electrochem: Comm.*, **12**, 820 (2010).
16. Timothy S. Arthur, Per-Anders Glans, Masaki Matsui, Ruigang Zhang, Biwu Ma, and Jinghua Guo, *Electrochem. Commun.*, **24**, 43 (2012).
17. Artur Braun, Kevin Sivula, Debajeet K. Bora, Junfa Zhu, Liang Zhang, Michael Gratzel, Jinghua Guo, and Edwin C. Constable, *J. Phys. Chem. C*, **116**(32), 16870 (2012).
18. S. Reich, C. Thomsen, and J. Maultzsch, *Carbon nanotubes*. Weinheim: Willey-VCH Verlag, (2004).
19. Y. Wang, D. C. Alsmeyer, and R. L. McCreery, *Chem. Matter*, **2**(5), 557 (1990).
20. A. Kaniyoor and S. Ramaprabhu, *AIP Adv.*, **2**, 032183 (2012).
21. A. Ismach, C. Druzgalski, S. Penwell, A. Schwartzberg, M. Zheng, A. Javey, J. Bokor, and Y. Zhang, *Nano Lett.*, **10**(5), 1542 (2010).
22. Y. Zhang, T. Gao, Y. Gao, S. Xie, Q. Ji, and K. Yan, *ACS Nano*, **5**(5), 4014 (2011).
23. J. Sik, K. Jin-Soo, B. Ik-Su, L. Duk-Hyun, L. Mi-Jung, and P. Bae-Ho, *Sci.*, **333**(6042), 607 (2011).
24. M. S. Dresselhaus and P. C. Eklund, *Adv. Phys.*, **49**(6), 705 (2000).

25. D. A. Fischer, R. M. Wentzcovitch, R. G. Carr, A. Continenza, and A. J. Freeman, *Phys. Rev. B*, **44**, 1427 (1991).
26. J. Robertson, *Mat. Sci. and Eng.*, **37**, 129 (2002).
27. S. Stasio and A. Braun, *Energy Fuels*, **20**(1), 187 (2006).
28. J. A. Horsley, J. Stöhr, A. P. Hitchcock, D. C. Newbury, A. L. Johnson, and F. Sette, *J. Chem. Phys.*, **83**, 6099 (1985).
29. H. K. Jeong, H. J. Noh, J. Y. Kim, M. H. Jin, C. Y. Park, and Y. H. Lee, *EPL*, **82**, 67004 (2008).
30. L. G. Cançado, K. Takai, T. Enoki, M. Endo, Y. A. Kim, H. Mizusaki, A. Jorio, L. N. Coelho, R. Magalhães-Paniago, and M. A. Pimenta, *Appl. Phys. Lett.*, **88**, 163106 (2006).
31. J.-P. Tessonnier, D. Rosenthal, T. W. Hansen, C. Hess, M. E. Schuster, R. Blume, F. Girgsdies, N. Pfänder, O. Timpe, D. S. Su, and R. Schlögl, *Carbon*, **47**(7), 1779 (2009).
32. D. J. Cott, M. Verheijen, O. Richard, I. Radu, S. De Gendt, S. van Elshocht, and P. M. Vereecken, *Carbon*, **58**, 59 (2013).
33. M. Miranda-Hernadez, J. A. Ayala, and M. E. Rincon, *J. Solid Statate Electrochem*, **7**, 264 (2003).
34. N. Behabtu, J. R. Lomeda, M. J. Green, A. L. Higginbotham, A. Sinitskii, D. V. Kosynkin, D. Tsentalovich, A. N. G. Parra-Vasquez, J. Schmidt, E. Kesselman, Y. Cohen, Y. Talmon, J. M. Tour, and M. Pasquali, *Nature Nanotechnology*, **5**, 406 (2010).
35. E. Hollauer, E. Prucole, M. Rocco, A. Netto, A. Schöll, and R. Fink, *J. Braz. Chem. Soc.*, **1**(1), (2005).
36. K. Suenaga and M. Koshino, *Nature*, **468**, 1088 (2010).
37. P. Skytt, P. Glans, D. C. Mancini, J. H. Guo, N. Wassdahl, and J. Nordgren, *Phys. Rev. B*, **50**(15), 10457 (1994).
38. T. Ito, L. Sun, and R. M. Crooks, *Electrochemical and Solid-State letters*, **6**(1), C4 (2003).
39. H. S. Choo, T. Kinumoto, Y. Iriyama, T. Abe, and Z. Ogumi, *ECS Transactions*, **11**(1), 1003 (2007).
40. E. Frackowiak, K. Metenier, V. Bertagna, and F. Beguin, *APL*, **77**, 2421 (2000).